Optical Engineering

OpticalEngineering.SPIEDigitalLibrary.org

Highly miniaturized endoscopic spatial confocal point distance sensor

Korbinian Prause
Simon Thiele
Alois M. Herkommer
Harald Giessen
Bernd Pinzer
Michael Layh

Korbinian Prause, Simon Thiele, Alois M. Herkommer, Harald Giessen, Bernd Pinzer, Michael Layh, "Highly miniaturized endoscopic spatial confocal point distance sensor," *Opt. Eng.* **59**(3), 035102 (2020), doi: 10.1117/1.OE.59.3.035102

Highly miniaturized endoscopic spatial confocal point distance sensor

Korbinian Prause,[a,b,*] Simon Thiele,[b] Alois M. Herkommer,[b] Harald Giessen,[c] Bernd Pinzer,[a] and Michael Layh[a]

[a]University of Applied Sciences Kempten, Laboratory for Optical 3D Metrology and Computer Vision, Kempten, Germany

[b]University of Stuttgart, Institute of Applied Optics and Research Center SCoPE, Stuttgart, Germany

[c]University of Stuttgart, 4th Physics Institute and Research Center SCoPE, Stuttgart, Germany

Abstract. We present a highly miniaturized endoscopic point distance sensor based on a spatial confocal measurement principle.[1] The sensor uses a new technique called spatial confocal point distance measurement. A special feature of the proposed sensor design is the high degree of miniaturization through femtosecond direct laser writing and the use of optical fiber bundles, which enable an endoscopic application. We show the complete sensor measurement principle, sensor head design, experimental setup, and experimental results. © *2020 Society of Photo-Optical Instrumentation Engineers (SPIE)* [DOI: 10.1117/1.OE.59.3.035102]

Keywords: micro-optics; image fiber; endoscopic sensor; miniaturization; three-dimensional printing; *in-situ* metrology; optical metrology; confocal; point distance sensor.

Paper 191323 received Sep. 19, 2019; accepted for publication Mar. 2, 2020; published online Mar. 17, 2020.

1 Introduction

Modern industrial manufacturing technology exhibits an increasing demand for highly miniaturized optical metrology systems and inspection tools. On the one hand, there still is a high demand for precision manufacturing even in hard-to-reach places, e.g., the inner surface of deep bore holes. The inspection of those hard-to-reach places with standard optical metrology methods can pose extreme difficulty or even be impossible. In addition, as additive manufacturing gains more and more industrial applications, the complexity of future components will increase.

On the other hand, there is a sustained trend toward inline inspection of the manufacturing process itself. But due to spatial limitations within modern manufacturing machines, an optical inspection becomes difficult or even impossible in the direct vicinity of the manufacturing tool itself.

Highly miniaturized endoscopic optical imaging and three-dimensional (3-D) metrology systems are able to reach these inaccessible regions and enable the inspection or metrology of these 3-D printed cavities or bore holes. In recent years, significant progress has been achieved in the field of additive manufacturing of micro-optics. Femtosecond direct laser writing[2–4] or multiphoton lithography has enabled the manufacturing of a wide variety of highly miniaturized micro- and nano-optical components with a very high degree of freedom and accuracy. It has been shown that femtosecond direct laser writing is a suitable tool for the manufacturing of various micro-optical components, ranging from optical components,[5–11] such as phase masks, waveguides, simple free form surfaces, and single microlenses, to rather complex optical systems, such as multilens systems[12–16] directly printed on top of optical fibers or image sensors. In this work, we take a look beyond beam shaping or imaging optics by utilizing the femtosecond direct laser writing technique to create a highly miniaturized optical point distance sensor. The proposed optical sensor is based on a spatial confocal measurement technique and is directly

*Address all correspondence to Korbinian Prause, E-mail: korbinian.prause@hs-kempten.de

placed at the end of a coherent fiber bundle and hence can also be used endoscopically. In Sec. 2, we introduce the basic idea of the spatial confocal point distance sensor and describe the detailed depth measurement process. In Sec. 3, we focus on the downscaling of the sensor to a diameter of about 600 μm, its adaptation with a coherent fiber bundle, and its optical design. The general data acquisition and calibration procedure will be illustrated in Sec. 4. Section 5 contains our experimental validation of the sensor concept, the experimental setup, the performance results, and discussion.

2 Spatial Confocal Measurement Principle

Chromatic confocal point distance sensors are well known and established in the field of surface metrology and allow, e.g., for surface topology and roughness measurements with a very high degree of accuracy and precision. The basic concept of a confocal point distance measurement is utilized in this sensor concept with the difference that the surface z-position is encoded into the spatial domain rather than the frequency or wavelength domain, as is the case with chromatic confocal point distance sensors.

The basic principle of the proposed spatial confocal point distance sensor is illustrated in Fig. 1. The beam of a monochromatic light source, shown in Fig. 1 as a green beam, is collimated with a very narrow and extended focus and is diffusely reflected at the surface of the test object. The distance z_o is defined as the distance from a reference point of the sensor assembly, e.g., the exit surface of the light source, to the test object surface.

A confocal sensor element CSE$_n$, consisting of an imaging lens L$_n$, a field stop FS$_n$ located at the image plane of the imaging lens, and an intensity sensor element IS$_n$, is now positioned some vertical distance away from the beam source. The tilt of the CSE$_n$ is adjusted in order to coincide the focal plane of the CSE with the illumination beam optical axis at the desired confocal distance z_n. Owing to the angle between the illumination beam axis and the CSE$_n$'s optical axis, spatial confocality is achieved in the intersection of both optical axes and is defined as the confocal plane. For a single CSE, this will yield a z_0-intensity distribution for different test object surface positions z_o that will reach a maximum if the test object surface is coincident with the confocal plane of the CSE, as shown for IS$_1$ in Fig. 1. To measure the surface z_o position of a test object surface with a single CSE, either the whole sensor assembly or the test object would have to be scanned along the z axis and the intensity recorded for different z_o positions. Through peak detection of the recorded intensity distribution the surface position can be determined.

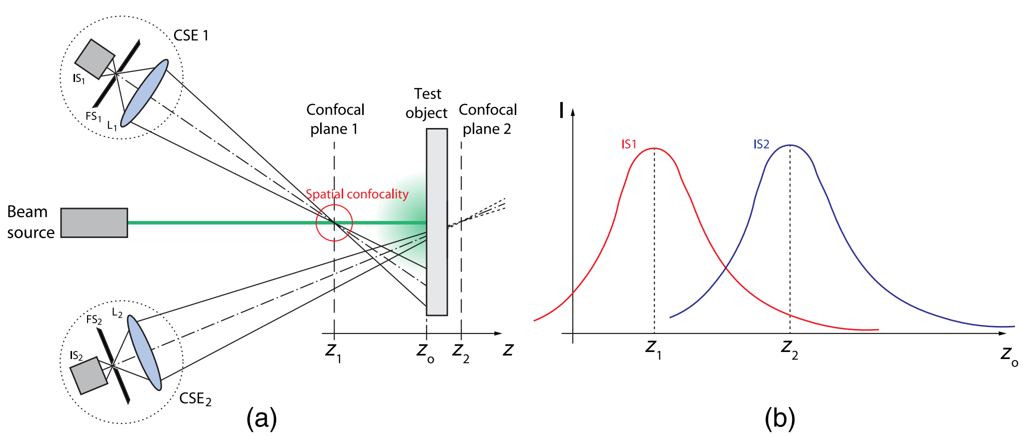

Fig. 1 Spatial confocal measurement principle: (a) Schematic representation of the proposed spatial confocal point distance measurement method. A collimated beam, shown as a green light beam, reflects from a test object. The scattered light is being imaged by several confocal sensor elements (CSE$_n$), consisting of an imaging lens (L$_n$), a field stop (FS$_n$), and an intensity sensor (IS$_n$). (b) A sketch of the recorded intensity distribution for the two shown CSEs for the intensity sensors IS$_1$ and IS$_2$, respectively, as a function of the test object position z_0.

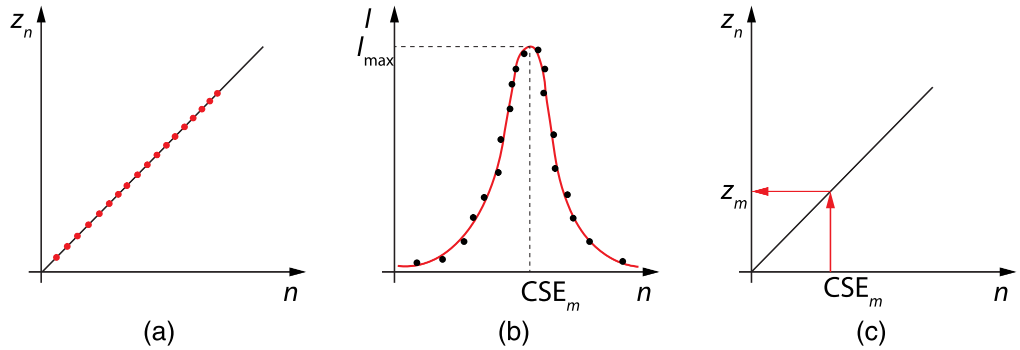

Fig. 2 Depth measurement procedure: (a) Depth information encoded into the axial confocal plane position z_n of each individual, (b) recorded CSE intensity distribution during a single-shot measurement, and (c) extraction of depth information by correlating peak intensity position n_m to encoded z position z_m lens with number n.

The necessity of a scanning component during the confocal point distance measurement can be eliminated by using multiple CSEs with different confocal planes. The actual number of CSEs depends on the total measurement range and the desired resolution of the z distance measurements, but for simplicity, only two CSEs are shown in Fig. 1. Let z_1 be the confocal plane position for CSE$_1$ and z_2 the confocal plane position for CSE$_2$, then the z_0-intensity distribution will reach a maximum for each intensity sensor IS$_1$ and IS$_2$ if the corresponding confocal plane is coincident with the test object surface.

Figure 2 illustrates the depth measurement process utilizing multiple CSEs located around the beam source, as illustrated in Fig. 1. Depth information is encoded by the position of the confocal planes z_n of different CSE$_n$. The axial confocal plane position z_n can be designed to have a linear relation to the CSE$_n$ element number n, as depicted in Fig. 2(a). Recording the intensity of each CSE$_n$ for a given test object surface position z_m will yield the CSE$_n$ intensity distribution depicted in Fig. 2. Since the relation between confocal plane position z_n and CSE$_n$ is known, the surface height can be determined through intensity peak CSE$_m$ detection in the recorded intensity distribution and calculation of the surface height through a linear curve fit of the CSE$_n$ − z_n distribution. In short, we can measure the test surface position by utilizing multiple CSEs with different known confocal plane positions distributed along the z_o axis and recording the intensity distribution across those CSEs with a single measurement.

3 Sensor Head Design

The miniaturization of the spatial confocal point distance measurement principle shown in Fig. 1 is made possible through the utilization of a coherent optical fiber bundle in combination with femtosecond direct laser writing. A coherent fiber bundle consists of thousands of single optical fibers arranged coherently to form a multicore image fiber. Each fiber within the fiber bundle can be illuminated individually, and therefore, multiple spatially separate channels can be used to transmit intensity information.

Figure 3(a) shows a side view of the optical sensor head. The central fiber core of the coherent fiber bundle acts as the illumination channel and the central aspheric lens is used to create a narrow beam (solid red line) with an extended depth of field. The individual confocal spatial sensor element consisting of an imaging lens, a field stop, and an intensity sensor, is replaced by a single tilted aspheric lenslet for each confocal plane distance. As depicted in Fig. 3(a), the aspheric imaging lenslet will perform two tasks, namely, imaging a confocal plane at distance z_n onto the fiber bundle end surface and coupling the reflected light into the corresponding fiber core. The field stop of the CSE is naturally replaced by the diameter of a single fiber core and will act as a field stop and limit the field of view of each lenslet to the desired area on the confocal plane. With this principle design, a light source can be coupled directly into the central fiber of the coherent fiber bundle and generate the illumination beam necessary. The light is then again reflected from a test object surface and the intensity is, according to the spatial confocal

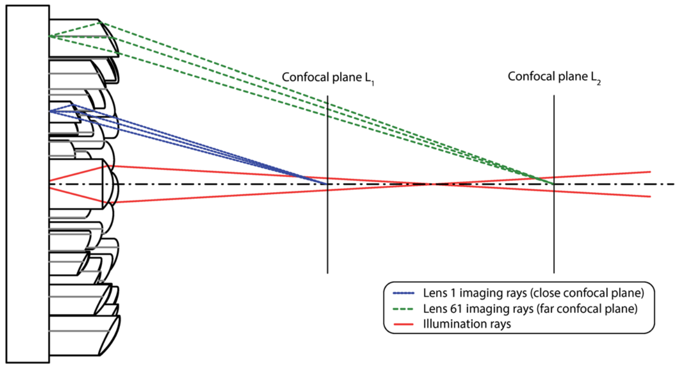

(a) Side view

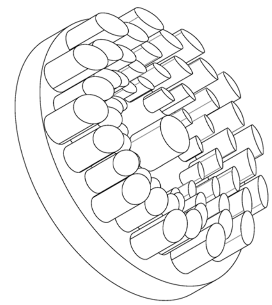

(b) Sensor head design

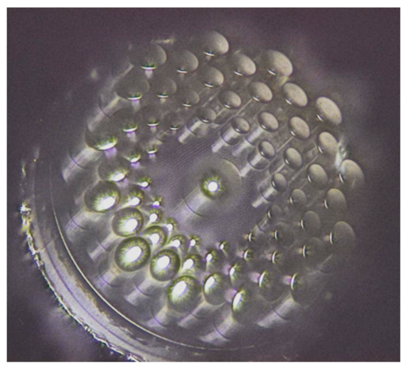

(c) Sensor head microscope image

Fig. 3 Sensor head design: (a) Side view of sensor head optical design. Each lens is individually optimized to image the center of a confocal plane L_m onto an individual fiber core of the coherent fiber bundle. The NA and magnification of each lens, as well as the angle between the imaging and illumination optical axes, are kept constant; (b) 3-D view of the sensor head assembly, with all lenses arranged around the central illumination lens; and (c) microscope image of the through femtosecond direct laser writing 3-D printed sensor head.

principle, transmitted by the fiber core located directly under the center of each imaging lenslet. By imaging the proximal end of the coherent fiber bundle, the intensity of the individual confocal lenslets can be recorded and the surface height calculated. The sensor head design shown in Fig. 3 consists of 61 individual confocal lenslets with confocal plane positions evenly distributed across a measurement range of 300 μm and a working distance away from the last surface of the sensor head of 500 μm aiming for a resolution of about ± 5 μm.

The micro-optical system described is designed, optimized, and simulated within the optical design software Zemax OpticStudio. The confocal lenslets, as shown in Fig. 3(c), consist of an aspheric surface with an added Zernike tilt term to compensate for off-axis imaging. In addition, the numerical aperture (NA) and magnification for each lenslet have been kept constant for the corresponding confocal plane position L_n. This results in different lens diameters and thicknesses, which can be seen in Fig. 3(b). The illumination lens has been optimized with an aspheric lens to compensate for spherical aberrations. Each lens has been individually optimized and its geometry is exported into a standard triangulation language (STL) file. Subsequently, the individual lenses are imported into a computer-aided design assembly and arranged according to their corresponding positions and design parameters. An additional bottom layer of filling material was added for increased support of individual lenses. The complete assembly is exported into an STL file.

The complete optical system is fabricated by 3-D dip-in direct laser writing using a commercially available femtosecond laser lithography system (Photonic Professional GT, Nanoscribe GmbH, Germany) and printed onto an optical fiber bundle. The whole micro-optical system is manufactured using a single material, a photoresist with high optical quality (IP-S, Nanoscribe GmbH).

4 Data Acquisition and Calibration

4.1 *Data Acquisition*

The signal of interest for the spatial confocal measurement principle, as shown in Fig. 1, is the light intensity imaged onto the intensity sensor of the CSEs. For the adaption of the spatial confocal measurement principle to a coherent optical fiber bundle, the field stop and intensity sensor are combined and replaced by a single fiber core of the fiber bundle. Hence it is necessary to record the light intensity that is transmitted by the fiber core that is located at the center of one CSE imaging lenslet.

Figure 4(a) shows the distribution of 61 lenslets, including the illumination lenslets in the center on the optical fiber bundle, starting with lenslet 1 at the innermost position and stopping with lenslet 61 on the outermost position. Ideally, each lenslet would be located such that a single fiber core is located at the center of the lenslet. Owing to limited access to the direct laser writing fabrication machine software, we were not able to individually place each lenslet at the ideal position. Therefore, the intensity values for each pixel within a small area at the center of each lenslet, as depicted in Fig. 4(b), have been extracted and stored. Furthermore, additional regions of interest (ROIs), as depicted in Fig. 4(b), can be used to subsample the measurement range with artificial measurement points. Unfortunately, this has not yielded an improvement in calibration or measurement quality, and therefore, has not been displayed in this work.

4.2 *System Calibration*

Figure 5(a) shows the raw z-lens-intensity distribution after conducting a scan of the test object surface along the z axis. As can clearly be seen, the recorded intensities vary a lot from lens to lens. Therefore, the individual lens intensity distributions (horizontal slices along the y axis) are normalized individually, as seen in Fig. 5(b). It can now be seen that due to manufacturing tolerances and the missing alignment to the central fiber cores, the lens order is not sorted. Therefore, the individual lenses are sorted according to their intensity peak positions, and a sorted z-lens-intensity distribution can be obtained, as illustrated in Fig. 5(c).

To be able to measure the position of a test surface along the z axis, a correspondence between a z position and the peak position of the measured signal along the lenslet intensities, as shown in Fig. 6(b), has to be determined. Therefore, a calibration scan, as shown in Fig. 6(a), was performed and the lens peak position, as in Fig. 6(b), for each z position has been determined. The correspondence between the stage z position and the lens peak position can be seen in Fig. 6(c). Only taking the ROI between 300 and 600 μm into account, a linear or 13th-order polynomial fit can be performed and a calibration curve extracted.

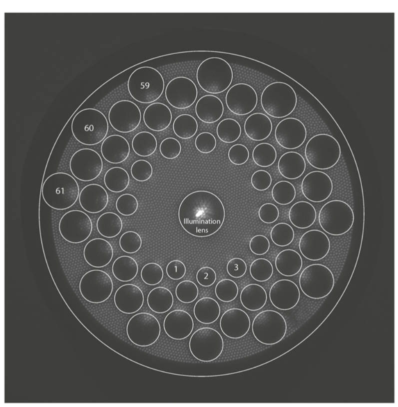

(a) Lenslet position

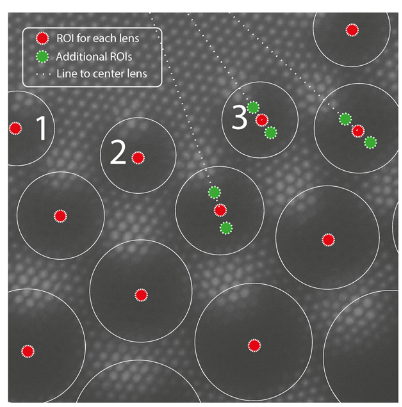

(b) ROI in lenslets

Fig. 4 Acquisition: (a) Lenslet position and numbers on the optical coherent fiber bundle and (b) ROI for intensity acquisition within the individual lenslets. Additional ROIs for subsampling of measurement range indicated.

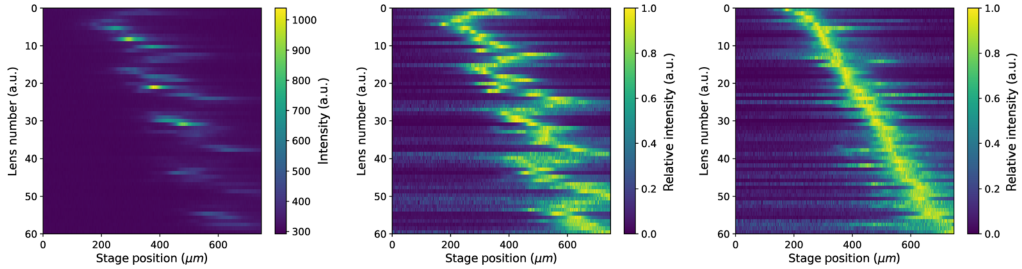

(a) Raw (b) Normalized (c) Sorted

Fig. 5 Calibration part I: (a) Raw z-lens-intensity distribution for z scan; (b) normalized z-lens-intensity distribution; and (c) normalized and sorted z-lens-intensity distribution.

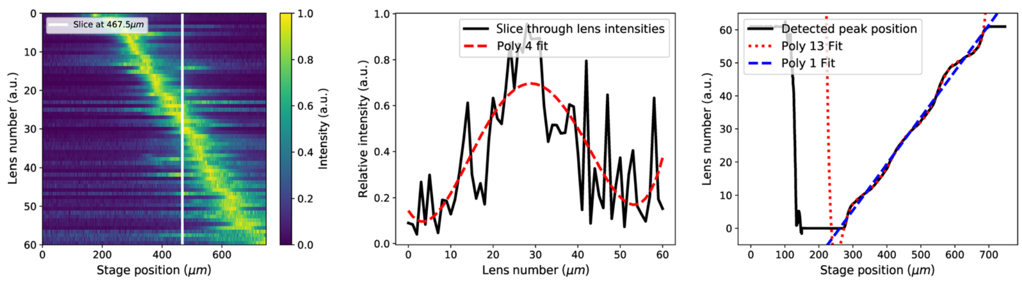

(a) Calibration scan (b) Calibration slice (c) Calibration curve

Fig. 6 Calibration part II: (a) Sorted z-lens-intensity distribution for z scan with slice indicated at 467.5 μm. (b) Slice of z-lens-intensity distribution with fourth-degree polynomial fit to determine the peak position. (c) Extracted peak positions for different stage positions with overlaid linear and 13th-degree polynomial fit to generate a calibration curve.

While a first-degree polynomial fit (linear fit) has been used for the following performance analysis, no significant decrease or increase in accuracy and repeatability has been found by fitting a polynomial with a higher degree. Both the 1st- and 13th-degree polynomial fits are shown in Fig. 6(c).

5 Experimental Results and Discussion

5.1 *Experimental Setup*

Figure 7 illustrates a schematic diagram of the experimental setup for the miniaturized endoscopic spatial confocal point distance sensor head. A spatial filter consisting of a lens doublet comprises a hybrid aspheric lens (#65-991, Edmund Optics), a PCX lens (#32-477, Edmund Optics), and a 20-μm pinhole is used to extract the TEM00 Mode from the light cone emitted by the TO Can Laser Diode (PL520, Thorlabs) used as a light source. The diverging beam is then collimated by a PCX lens (#33365, Edmund Optics). The collimated beam is then reflected by a tip-tilt mirror assembly comprising a standard 1-inch mirror mount (KS1, Thorlabs) with motorized adjustment screws (PIAK10, Thorlabs) and a standard 1-inch mirror (#64-015, Edmund Optics), which enables precise scanning motion in the x and y directions. The beam then passes through a nonpolarizing beam splitter (NPBS, #32-505, Edmund Optics). The unused side of the beam splitter is blocked with a beam dump. After the beam exits the beam splitter, it is focused onto the proximal end of the coherent fiber bundle (FIGH-10-500N, Fujikura) by a standard camera objective (#59-872, Edmund Optics).

The light coupled into the coherent image fiber by the coupling objective will travel through the fiber and be used by the miniaturized spatial confocal sensor head, as described in Fig. 3. Light reflected off the surface and coupled back into the coherent image fiber will again be collimated by the coupling objective and be reflected by the NPBS. An imaging objective

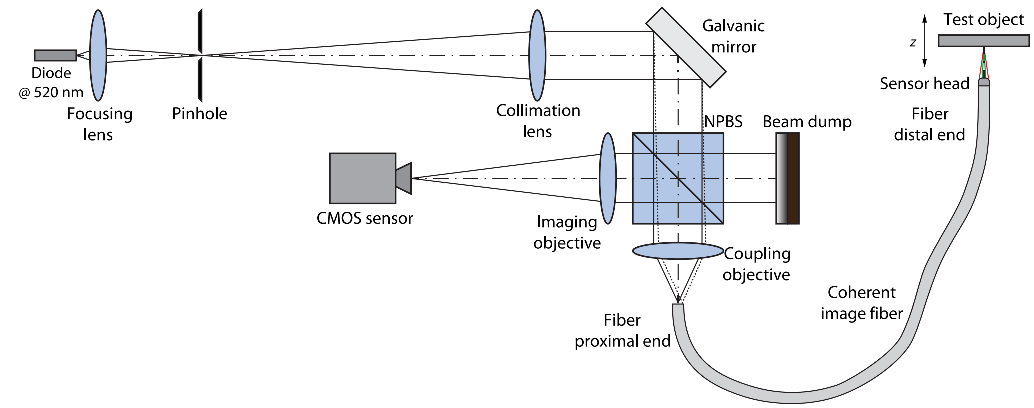

Fig. 7 Experimental setup. Schematic diagram of the experimental setup for the spatial confocal endoscopic sensor head. A 520-nm light source is spatially filtered to generate a collimated light beam that is positioned on the proximal end of the coherent fiber bundle with the use of a galvanic mirror. The reflected light of the test surface is then imaged using an imaging objective and a CMOS sensor.

(#32-325, Edmund Optics) will then form an image of the proximal fiber end on a commercial CMOS sensor (GS3-U3-50S5M-C, PointGrey). The image of the proximal end of the coherent fiber will then be used to analyze the recorded reflection of the spatial confocal sensor head on the distal end of the fiber bundle. The spatial confocal sensor utilizes a narrow band laser diode source. In this setup, we used a TO Can Laser Diode (PL520, Thorlabs), which is very inexpensive and offers a stable coherent light source at 520 nm. Since we are not able to use different types of materials for the 3-D printed micro-optics, as would be possible for conventional optic manufacturing, on the distal end of the coherent image fiber the limitation to a single wavelength will significantly simplify the optical design of the sensor head optics. To sustain a highly compact optical system that can transmit both the illumination and imaging part of the confocal system, a coherent fiber bundle (FIGH-10-500N, Fujikura) was used. The fiber bundle contains about 10,000 individual fibers with a single core diameter of 3 μm. The overall fiber diameter is 600 μm with an image circle diameter of 460 μm. The length of each fiber segment is 200 mm.

The surface sample to be measured has been positioned on a standard linear stage (XR25-C, Thorlabs) equipped with a piezoelectric inertia linear actuator (PIA25, Thorlabs), which offers a repeatable and accurate step size of 20 nm. The stage accuracy and repeatability has been tested with an interferometer before use in the test setup.

5.2 *Results and Discussion*

The system performance has been investigated for three different material surfaces. A diffuser surface (DG10-1500-P01, Thorlabs) has been used as a static and a dithered—the dithered movement has been achieved through mounting the diffusor on the end of stepper motor that has been controlled using a sinusoidal voltage with a frequency higher than the stepper motor can handle—target for the spatial confocal sensor head, as well as a static ground aluminum surface. For each surface, five depth scans have been performed by mounting the target on a translation stage and recording the intensity information of the sensor head for multiple stage positions. The sensor has been calibrated before the whole measurement sequence, according to the calibration procedure described in Sec. 4.2. Figure 8 shows the depth scans for each surface, with a calibrated sensor over the whole desired measurement range of 300 μm.

Figure 8 clearly shows considerable divergence around the desired linear position of the surface. It can also be observed that the divergence is reduced by substituting a ground aluminum surface for the dithered diffuser surface. In addition, a global offset of measured position in relation to desired position can be observed.

Removing the desired stage position offset, shown in Fig. 8 as a linear fit with a fixed slope of 1, the difference between the desired position and the actual stage position can be extracted, as

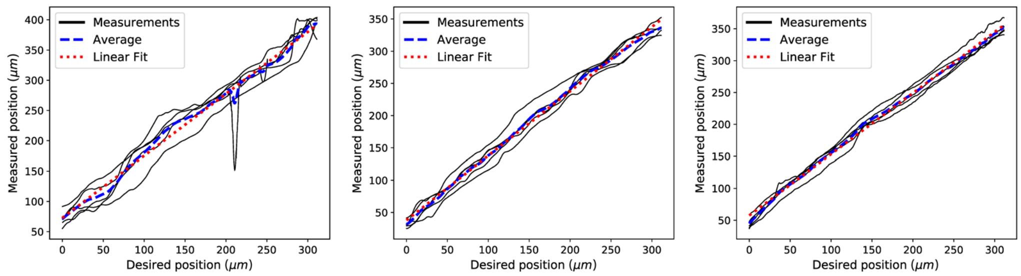

(a) Aluminum (b) Diffuser static (c) Diffuser dithered

Fig. 8 Test measurement scans. Depth scans for different test object surfaces. (a) Aluminum, (b) static, and (c) dithered diffuser.

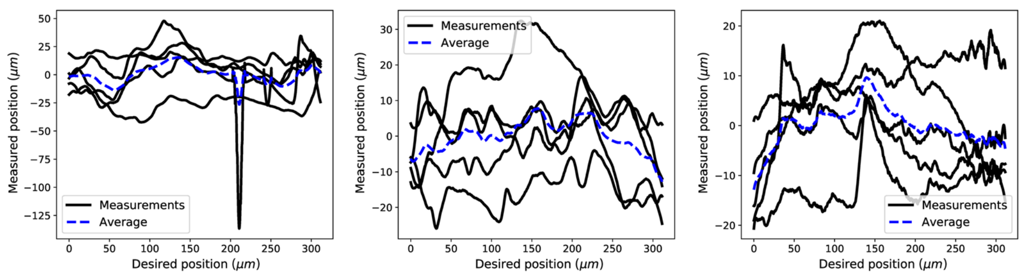

(a) Aluminum (b) Diffuser Static (c) Diffuser Dithered

Fig. 9 Test measurement differences. Differences of the measured position to the optimal desired position for different surfaces. (a) Aluminum, (b) static, and (c) dithered diffuser.

shown in Fig. 9. From there the root mean square (rms) and PV (peak-to-valley) values for each scan can be calculated and the performance of the sensor head determined. Table 1 shows the different rms and PV values for different test surfaces. It can be seen that for more uniformly scattering surfaces, the rms and PV values decrease, and therefore, the sensor head performance increases. It can also be clearly seen in Fig. 9 that a nonuniformly scattering surface such as aluminum can lead to large deviations in the measured position.

The core principle of this spatial confocal sensor head is to record the intensity of a light beam reflected off a test object. Unfortunately, the aluminum target reveals an inherent problem: The reflected intensity is directly dependent on the bidirectional reflectance function of the test object surface. For machined surfaces, the size of surface features and the surface roughness will even be in the same scale as the illumination spot, which will result in a direct dependency of local surface slope and reflectance angle. Therefore, a large NA would be necessary to capture all the reflected light. Because the available space on top of the fiber bundle is limited and multiple CSEs are necessary to adequately sample the whole range of measurement, only a very limited NA can be achieved for the individual CSE/lenslet. This will result in a slightly different z-intensity profile, and therefore, in a deviation in surface position calculation. A possible solution to this problem would be to reduce the number of CSEs and increase the diameter of each

Table 1 RMS and PV Values for Different Test Surfaces.

Material	rms (μm)	PV (μm)
Aluminum	13.7	182.2 (with artifacts)
		93.4 (without artifacts)
Diffuser static	7.7	57.7
Diffuser dithered	6.9	43.8

lens in order to increase the NA of the individual lenslets. At the same time, this would decrease the number of samples across the measurement range. Thus an optimal relation between number of CSEs and lenslet diameter has to be identified.

A second more promising solution would be to, rather than focusing on the reflected intensity for each lenslet, treat the individual lenslets and the illumination lenslet as a triangulation sensor. For this approach, the reflected intensity peak location on the fiber bundle for each lenslet in relation to the central illumination lenslet will be identified instead of the intensity itself. For that, multiple fiber cores are necessary. This will get rid of the surface roughness dependency and increase the robustness of the sensor head for nonuniformly scattering surfaces. This approach has already been tested in first tests with the current sensor head, and a more robust measurement and far easier calibration has been achieved, which we will report in a follow-up paper. Nevertheless, further improvements still have to be performed within the data-processing algorithms to achieve a greater robustness, namely peak detection and deconvolution of the fiber bundle core pattern.

6 Conclusion

In this work, we introduce a concept and experimental validation for a highly miniaturized spatial confocal point distance sensor through the combination of multiple freeform microlenses, femtosecond laser writing, and the use of coherent optical fiber bundles, an endoscopic sensor head concept with a diameter less than 600 μm, a measurement range of 300 μm at a working distance of 500 μm, and experimentally determined resolution of up to ± 6.9 μm rms.

Next steps will include the further optimization of the measurement process and elimination of the dependency to reflected light intensity and instead treat the sensor head as a triangulation sensor and extract the surface height information from the average radius of each lenslet intensity peak relative to the central illumination lenslet. We could demonstrate the principle with a perfect diffusor surface. However, further improvement is mandatory to make this sensor concept viable for use in industrial surface metrology applications.

Acknowledgments

K.P., M.L., and B.P. gratefully acknowledge financial support from EffPro—financed through the Europäischen Fond für regionale Entwicklung the European Union as well as the EFRE-Bayern and carried out by the University of Applied Sciences Kempten and the Bayrisches Staatsministerium für Unterricht und Kultus. H.G., A.H., and S.T. acknowledge funding by ERC-AdG (ComplexPlas), ERC-PoC (3D PrintedOptics), BW-Stiftung (Opterial), and BMBF (Printoptics and Printfunction).

References

1. K. Prause et al., “Concept for a highly miniaturized endoscopic point distance sensor,” *Proc. SPIE* **11056**, 110560M (2019).
2. M. Malinauskas et al., “Femtosecond laser polymerization of hybrid/integrated micro-optical elements and their characterization,” *J. Opt.* **12**(12), 124010 (2010).
3. R. Guo et al., “Micro lens fabrication by means of femtosecond two photon photopolymerization,” *Opt. Express* **14**(2), 810–816 (2006).
4. M. Farsari and B. N. Chichkov, “Materials processing: two-photon fabrication,” *Nat. Photonics* **3**(8), 450–452 (2009).
5. N. Lindenmann et al., “Photonic wire bonding: a novel concept for chip-scale interconnects,” *Opt. Express* **20**(16), 17667 (2012).
6. A. Žukauskas, M. Malinauskas, and E. Brasselet, “Monolithic generators of pseudo-nondiffracting optical vortex beams at the microscale,” *Appl. Phys. Lett.* **103**(18), 181122 (2013).
7. L. Li and A. Y. Yi, “Design and fabrication of a freeform prism array for 3D microscopy,” *J. Opt. Soc. Am. A* **27**(12), 2613–2620 (2010).

8. M. Deubel et al., "Direct laser writing of three-dimensional photonic-crystal templates for telecommunications," *Nat. Mater.* **3**(7), 444–447 (2004).
9. J. Dunkel et al., "Fabrication of refractive freeform array masters for artificial compound eye cameras," *Proc. SPIE* **9130**, 91300P (2014).
10. S. Thiele et al., "Ultra-compact on-chip LED collimation optics by 3D femtosecond direct laser writing," *Opt. Lett.* **41**(13), 3029–3032 (2016).
11. R. J. Winfield et al., "Fabrication of grating structures by simultaneous multi-spot fs laser writing," *Appl. Surf. Sci.* **253**(19), 8086–8090 (2007).
12. T. Gissibl et al., "Two-photon direct laser writing of ultracompact multi-lens objectives," *Nat. Photonics* **10**, 554–560 (2016).
13. S. Thiele et al., "3D-printed eagle eye: compound microlens system for foveated imaging," *Sci. Adv.* **3**(2), e1602655 (2017).
14. T. Gissibl et al., "Sub-micrometre accurate free-form optics by three-dimensional printing on single-mode fibres," *Nat. Commun.* **7**, 11763 (2016).
15. C. Liberale et al., "Micro-optics fabrication on top of optical fibers using two-photon lithography," *IEEE Photonics Technol. Lett.* **22**(7), 474–476 (2010).
16. Y. Choi et al., "Scanner-free and wide-field endoscopic imaging by using a single multimode optical fiber," *Phys. Rev. Lett.* **109**(20), 203901 (2012).

Biographies of the authors are not available.